Original research

Title: *MYCN de novo* gain-of-function mutation in a patient with a novel megalencephaly syndrome

Authors:

Kohji Kato[1,2], Fuyuki Miya[3,4], Nanako Hamada[5], Yutaka Negishi[1], Yoko Narumi-Kishimoto [6], Hiroshi Ozawa[6], Hidenori Ito[5], Ikumi Hori[1], Ayako Hattori[1], Nobuhiko Okamoto[7], Mitsuhiro Kato[8], Tatsuhiko Tsunoda[3,4], Yonehiro Kanemura[9,10], Kenjiro Kosaki[11], Yoshiyuki Takahashi[2], Koh-ichi Nagata[5], Shinji Saitoh[1]

[1]Department of Pediatrics and Neonatology, Nagoya City University Graduate School of Medical Sciences, Nagoya, Japan

[2]Department of Pediatrics, Nagoya University Graduate School of Medicine, Nagoya, Japan

[3]Department of Medical Science Mathematics, Medical Research Institute, Tokyo Medical and Dental University, Tokyo, Japan

[4]Laboratory for Medical Science Mathematics, RIKEN Center for Integrative Medical Sciences, Yokohama, Japan

[5]Department of Molecular Neurobiology, Institute for Developmental Research, Aichi Human Service Center, Kasugai, Japan

[6]Department of Pediatrics, Shimada Ryoiku Center Hachiouji, Tokyo, Japan

[7]Department of Medical Genetics, Osaka Women's and Children's Hospital, Osaka, Japan

[8]Department of Pediatrics, Showa University School of Medicine, Tokyo, Japan

[9]Division of Biomedical Research and Innovation, Institute for Clinical Research, Osaka National Hospital, National Hospital Organization, Osaka, Japan

[10]Department of Neurosurgery, Osaka National Hospital, National Hospital Organization, Osaka, Japan

[11]Center for Medical Genetics, Keio University School of Medicine, Tokyo, Japan

Correspondence: Shinji Saitoh, MD, PhD

Department of Pediatrics and Neonatology, Nagoya City University Graduate School of Medical Sciences

1 Kawasumi, Mizuho-Cho, Mizuho-Ku, Nagoya 467-8601, Japan

TEL: 81-52-853-8246 FAX: 81-52-842-3449

E-mail: ss11@med.nagoya-cu.ac.jp

Abstract

Background: In this study, we aimed to identify the gene abnormality responsible for pathogenicity in an individual with an undiagnosed neurodevelopmental disorder with megalencephaly, ventriculomegaly, hypoplastic corpus callosum, intellectual disability, polydactyly and neuroblastoma. We then explored the underlying molecular mechanism.

Methods: Trio-based whole-exome sequencing was performed to identify disease-causing gene mutation. Biochemical and cell biological analyses were carried out to elucidate the pathophysiological significance of the identified gene mutation.

Results: We identified a heterozygous missense mutation (c.173C>T; p.Thr58Met) in the *MYCN* gene, at the Thr58 phosphorylation site essential for ubiquitination and subsequent MYCN degradation. The mutant MYCN (MYCN-T58M) was non-phosphorylatable at Thr58 and subsequently accumulated in cells and appeared to induce CCND1 and CCND2 expression in neuronal progenitor and stem cells *in vitro*. Overexpression of Mycn mimicking the p.Thr58Met mutation also promoted neuronal cell proliferation, and affected neuronal cell migration during corticogenesis in mouse embryos.

Conclusions: We identified a *de novo* c.173C>T mutation in *MYCN* which leads to stabilization and accumulation of the MYCN protein, leading to prolonged CCND1 and CCND2 expression. This may promote neurogenesis in the developing cerebral cortex,

leading to megalencephaly. While loss-of-function mutations in *MYCN* are known to cause Feingold syndrome, this is the first report of a germline gain-of-function mutation in *MYCN* identified in a patient with a novel megalencephaly syndrome similar to, but distinct from, CCND2-related megalencephaly-polymicrogyria-polydactyly-hydrocephalus syndrome. The data obtained here provides new insight into the critical role of MYCN in brain development, as well as the consequences of MYCN defects.

Key words: neuroblastoma, polydactyly, missense mutation, neurogenesis, neurodevelopment

INTRODUCTION

The MYC transcription factor family targets proliferative and apoptotic pathways, and members of this family, *MYC*, *MYCL1*, and *MYCN*, are well established proto-oncogenes in humans[1]. *MYCN* amplification is found in about 25% of neuroblastoma cases, the most common malignant extracranial solid tumor in childhood[2]. *MYCN* also plays an important role in the early embryonic development of various organs, including the central nervous system, limb bud, lung, gut, and heart[3-6].

MYCN mRNA expression was reported to be high in fetal, but less so in adult, human brain[7]. Germline heterozygous loss-of-function mutations or microdeletions in *MYCN* are known to cause Feingold syndrome (MIM: 164280), which is characterized by microcephaly, learning disabilities and limb malformations[8, 9]. In the cerebellum, Mycn (murine orthologue) activity regulates granule neuron proliferation through induction of Ccnd1 and Ccnd2 (murine orthologues of human CCND1 and CCND2, respectively)[10]. While Mycn overexpression was shown to promote proliferation of granule neuron progenitor cells in cerebellum, its conditional loss of Mycn resulted in impaired proliferation of granule neuron progenitor cells, leading to reduced cerebellar mass[4]. Furthermore, *CCND2* gene abnormalities that impart excessive protein stability cause megalencephaly-polymicrogyria-polydactyly-hydrocephalus syndrome (MPPH; MIM: 615938)[11]. Notably,

CCND2 stability also appears to be augmented by other MPPH-associated mutations in *AKT3, PIK3R2*, and *PIK3CA*[12].

Phosphorylation of MYCN is crucial for its structural stability. It is stabilized and activated through phosphorylation of Ser62 (S62), which is followed by priming phosphorylation at Thr58 (T58)[13, 14]. Dephosphorylation of S62 then sensitizes T58-phospho-MYCN to interact with ubiquitin ligases such as F-box and WD repeat domain-containing 7 (FBW7), leading to proteasomal degradation[13, 15, 16]. S62 and T58 residues are highly conserved across all MYC family members, and frequently mutated in c-Myc in Burkitt's lymphoma, consistent with their functions in cell proliferation and differentiation[17].

Here we report a *de novo* heterozygous missense mutation in *MYCN* identified by whole-exome sequencing of a Japanese male with an intellectual disability (ID), distinctive facies, megalencephaly, ventriculomegaly, hypoplastic corpus callosum, postnatal growth retardation, postaxial polydactyly and neuroblastoma. Biochemical and cell biology experiments revealed that the mutation renders MYCN resistant to proteolysis and may improperly potentiate cortical neuron proliferation. We conclude that this mutation functions in a gain-of-function manner rather than the previously reported loss-of-function mutations that cause Feingold syndrome.

METHODS

Whole-exome analysis

Molecular diagnosis was performed using whole-exome sequencing on a patient with an increased head circumference and neurological symptoms, but with no mutations in 15 known megalencephaly genes[18]. The genomic DNA was extracted from peripheral blood, partitioned using the SureSelect XT Human All Exon V6 capture library (Agilent Technologies, Santa Clara, CA), and DNA sequencing was performed using 150-bp paired end reads with an Illumina HiSeq 4000 sequencer. To identify disease-causing mutations, we excluded variants with a minor allele frequency > 0.5 % in public databases and an in-house control database (1,044 controls of normal Japanese individuals and with other diseases), except those also identified as pathogenic mutations in the National Center for Biotechnology Information (NCBI) ClinVar and Human Gene Mutation Database (HGMD) databases. Public databases used were dbSNP150; 1,000 Genomes Project; Exome Aggregation Consortium (ExAC); National Heart, Lung, and Blood Institute Exome Sequencing Project 6500 (NHLBI ESP6500); Human Genetic Variation Database (HGVD); and the Integrative Japanese Genome Variation (iJGVD). We then excluded non-functional mutations to select nonsynonymous SNVs, insertions and deletions (indels) and splice site variants. The mutation was confirmed by Sanger sequencing of PCR-amplified products.

This study was approved by the Ethical Committee for the Study of Human Gene Analysis at Nagoya City University Graduate School of Medical Sciences. Written informed consent was obtained from the parents.

Plasmids

Mouse *Mycn* was amplified by RT-PCR from pooled adult mouse brain RNA, and the cDNA was cloned into the pCAG-Myc vector (Addgene Inc., Cambridge, MA). pCDNA3-hemagglutinin (HA)-tagged human MYCN was obtained from Addgene (plasmid #71463). Site-directed mutagenesis (KOD-Plus Mutagenesis Kit, Toyobo, Osaka, Japan) was then used to generate Mycn-T58M, MYCN-T58M, and MYCN-P44L mutant constructs from pCAG-Myc-Mycn and pCDNA3-HA-MYCN, respectively. Mouse Fbw7 cDNA, a kind gift from Prof. K. Nakayama (Kyushu University, Fukuoka, Japan), was cloned into the pCAG-Myc vector. All constructs were verified by DNA sequencing.

Cell culture

HEK293T cells were cultured and transfected with Lipofectamine 3000 (Life Technologies Japan, Tokyo) according to the manufacturer's guidelines. Mouse neuronal stem cells were isolated from embryonic day (E) 14 embryos and kept in the growth medium with basic

fibroblast growth factor, B27 and epidermal growth factor (Thermo Fisher Scientific) supplement. Primary neurospheres were dispersed with 0.2% trypsin, and cells were electroporated with a CUY21 electroporator (NEPA Gene, Chiba, Japan), according to the manufacturer's guidelines.

Preparation of mouse whole-brain extracts

Brains at various developmental stages were homogenized with 10 volumes of 50 mM Tris-HCl buffer (pH 7.5) containing 0.1 M NaF, 5 mM EDTA, 2% sodium dodecyl sulfate (SDS), 10μg/ml aprotinin and 10μg/ml leupeptin[19]. Protein concentration was estimated with a micro bicinchoninic acid (BCA) protein assay kit (Thermo Fisher Scientific) with bovine serum albumin as a standard.

Western blot

Indicated amounts of tissue or cell extracts were separated by SDS-PAGE (10% gel) and transferred to polyvinylidene difluoride (PVDF) membranes (Millipore, Billerica, MA). After blocking with 5% skim milk powder, membranes were incubated with primary antibodies against N-Myc (sc-53993; Santa Cruz Biotechnology, Texas, USA), phospho-c-Myc (pThr58) (ab28842; Abcam, Cambridge, UK), phospho-n-Myc (S54) (Bethyl labs,

Montogomery, TX), CCND1 (sc-450; Santa Cruz Biotechnology), CCND2 (ab 3085; Abcam), GFP (sc-9996; Santa Cruz Biotechnology), Myc-tag (#562; MBL, Nagoya, Japan), and GAPDH (#5174; Cell Signaling Technology, Danvers, USA), followed by incubation with horseradish peroxidase–conjugated secondary antibody (GE Healthcare, Little Chalfont, UK). Densitometric quantification was performed using ImageJ software.

In utero electroporation and EdU incorporation experiments

In utero electroporation was performed with pregnant ICR mice as previously described[20], with the following amendments. Embryos were electroporated with pCAG-EGFP together with pCAG-Myc-Mycn or the pCAG-Myc control vector at E14.5. 5-ethynil-2'-deoxyuridine (EdU) injection (25 mg/kg body weight) was performed at 24 h, then at 48 h brains were processed for sectioning and staining for EdU, Ki67 and GFP. The ratio of EdU/Ki67/GFP triple-positive cells to EdU/GFP double-positive ones was determined.

Quantitative analysis of neuronal migration

Distribution of GFP-positive cells in the coronal sections were quantified by calculation of the number of labeled cells in each region of the brain slices [21] .

Statistical analysis

Results are presented as the mean ± standard error of the mean (s.e.m). Two-sided Student's *t*-test was performed to compare the means between two groups. When the

means of three groups were to be compared, one-way ANOVA with post hoc Tukey's Honestly Significant Difference Calculator test was used. Statistics were calculated using EZR (Saitama Medical Center, Jichi Medical University, Saitama, Japan)[22]. $P < 0.05$ was considered significant.

RESULTS

Clinical findings

The subject of this study was a 15-year-old male, the second son of unrelated and healthy Japanese parents. He was born at 36 weeks gestation with a birth weight of 2915 g (82th percentile), length of 48 cm (74th percentile), and head circumference of 35 cm (97th percentile). He was admitted to a neonatal intensive care unit because of multiple congenital anomalies, including ventricular septal defect, tracheomalacia, and eventration of diaphragm. He gradually presented with respiratory distress and was intubated 40 days after birth with a subsequent tracheotomy performed at 3 months of age. At seven months of age he was diagnosed with stage 4S neuroblastoma originating from the sympathetic nerve ganglia in his abdomen with lower limb metastasis[23], and attained remission with extirpative surgery and chemotherapy. He presented with postnatal growth retardation and megalencephaly, with a height of 146 cm (−3.4 SD), body weight of 30 kg (−2.6 SD), and head circumference of 62 cm (+5.9 SD) at 15 years of age. He had facial dysmorphic features of prominent forehead, thick and laterally extended eyebrow, posteriorly rotated ear, epicanthus, hypertelorism, wide and depressed nasal bridge, wide nasal base, upturned nasal tip, long philtrum, square face, and high arched palate (Fig.1A-B). He had postaxial polydactyly of hands and feet (Fig.1C). His global development was delayed with

a total developmental quotient (Kinder Infant Developmental Scale[24]) of 12 at 6 years of age. Developmental regression was not observed, and he was able to walk alone and speak several single words at the latest visit. Brain magnetic resonance imaging (MRI) showed ventriculomegaly and hypoplastic corpus callosum, but no cortical dysplasia like polymicrogyria (Fig.1D-F). He developed generalized epilepsy at 10 years of age, which has been controlled by administration of zonisamide.

Genetic findings

To identify the causative mutation underlying the patient's phenotype, we performed trio-based whole-exome sequence (Fig.2A-B). Total reads by exome sequencing ranged from 54.0M to 65.8M reads (8.1G to 9.9G bases), and the mean depth at the target region was 81.8× to 100.4×. Following filtering, seven candidate genes remained: four *de novo* mutations, one associated with an autosomal recessive trait, and two associated with X-linked recessive traits (Fig.2A). After prioritization, a *de novo* heterozygous missense mutation (NM_005378.5; c.173C>T; p.Thr58Met) in the *MYCN* gene was identified as the top candidate, which was confirmed by Sanger sequencing (Fig.2C). It is noteworthy that the missense mutation was not listed in any public databases of general population (e.g. ExAC), although it was present in COSMIC database, somatic gene alterations in cancer.

In addition, Thr58 residue is evolutionally conserved (Fig.2D). Indeed, the mutation was predicted to be pathogenic and damaging by *in silico* analyses (Polyphen-2: score = 1.000, SIFT: score = 0.02, and CADD phred-score = 33).

Developmental changes of Mycn expression

Analysis of *MYCN* mRNA expression during fetal human brain development found it was highly expressed in immature neuronal cells, but this expression decreased after terminal differentiation[7]. Only fragmentary information is available, however, for mouse Mycn protein expression during brain development. Thus, to better understand the role of Mycn in neuronal development, we examined the temporal expression pattern of Mycn in whole-tissue extracts of mouse brains at various developmental stages. Mycn (~65 kDa) was highly expressed at E13.5, then gradually decreased to its lowest level by postnatal day (P)15 (Fig.3). Sept11, a cytoskeleton-related protein, was visualized as a loading control (Fig.3). This result confirmed that the temporal expression pattern of Mycn protein in the mouse brain reflected the situation in humans, and suggests Mycn plays an important role in brain development.

Effect of the c.173C>T mutation upon Mycn stability and Ccnd1/2 expression

As the identified missense mutation c.173C>T occurs at T58, phosphorylation of which is crucial for MYCN degradation in neuronal precursor cells[25], we hypothesized the mutant MYCN-T58M protein accumulates due to being constitutively non-phosphorylatable. To test this possibility, we over-expressed MYCN-T58M and wild-type MYCN in HEK293T cells. We also over-expressed MYCN-P44L, which is the most common missense mutation of *MYCN* according to the COSMIC cancer cell database. While the expression of total MYCN was comparable between HEK293T cells expressing wild-type MYCN and MYCN-T58M, the antibody against T58-phosphorylated MYC showed negligible T58 phosphorylation in MYCN-T58M compared with wild-type MYCN. In addition, we observed an increased level of phosphorylation at T58 and S62 in MYCN-P44L compared to wild-type (Fig.4A, one-way ANOVA with post hoc Tukey's Honestly Significant Difference Calculator test; DF = 2, F = 59.2, $P < 0.01$ for p-T58/MYCN; DF=2, F = 8.42, $P < 0.05$ for p-S62/MYCN). These results suggest the possibility that mutations affecting the phosphorylation state at T58 or S62 change the biological activity of MYCN.

Next, to assess the pathophysiological significance of the mutation in brain development we analyzed the effect of the p.T58M mutation on protein stability in neuronal progenitor/stem cells. When pCAG-Myc-Mycn or pCAG-MYC-Mycn-T58M were electroporated into neurosphere cells with or without pCAG-Myc-Fbw7 (ubiquitin

ligase[16]), Mycn-T58M was shown to be more stable than wild-type Mycn 24 h after electroporation (Two-sided Student's *t*-test; $P < 0.01$ for Fbw7+, $P = 0.045$ for Fbw7-; statistical analysis was run separately for Fbw7+ and Fbw7-) (Fig.4B). Degradation of Mycn was much more prominent when the ubiquitin-proteasome system was enhanced by coexpression of Fbw7 (Fig.4B), thus, subsequent experiments were performed with Fbw7 coexpression. Seventy-two hours after electroporation, Mycn-T58M was still expressed at high levels, approximately eight times higher than wild-type Mycn (8.6 ± 1.5 (mean ± s.e.m.), $P < 0.01$) (Fig.4C). These results support the hypothesis that the non-phosphorylatable c.173C>T mutation confers resistance to ubiquitin-proteasome-mediated degradation of Mycn.

We next asked whether the p.T58M mutation affects neuronal cell proliferation. To this end, we prepared neuronal progenitor/stem cells, and assessed the expression levels of Ccnd1 and Ccnd2, *Mycn* target gene products that promote cellular division and proliferation[26-28]. As shown in Fig.4D, overexpression of both Mycn-T58M and wild-type Mycn induced expression of Ccnd1 and Ccnd2, but significantly higher expression was observed in cells expressing Mycn-T58M (one-way ANOVA with post hoc Tukey's Honestly Significant Difference Calculator test; DF = 2, $F = 19.5$, $P < 0.01$ for Ccnd1; DF=2, $F = 43.9$, $P < 0.01$ for Ccnd2. Expression level was normalized to Gapdh). We co-transfected GFP to check

the proportion of transfected cells because excess expression of Mycn was reported to cause apoptosis [29] [30]. We confirmed that the same amount of GFP is expressed at 24 h after transfection (Supplementary Fig.1). However, overexpression of both wild-type Mycn and Mycn-T58M decreased expression level of GFP, and cells with Mycn-T58M were strongly affected than wild-type Mycn 72 h after transfection (Fig.4D), indicating putative cell death induced by overexpression of wild-type Mycn or Mycn-T58M. Therefore, overexpression of wild-type Mycn or Mycn-T58M induces bidirectional effects on neuronal cell proliferation and apoptosis, and Mycn-T58M showed strong effects on both cellular events.

Effect of Mycn expression on neuronal progenitor/stem cell proliferation and migration

Amplification of *MYCN* is found in about 25% of cases of neuroblastoma, which originates from undifferentiated neuronal crest cells. Megalencephaly associated with *CCND2* gene abnormalities is thought to be caused from dysregulation of neuronal progenitor cell cycle, which increases their cell numbers[11]. So far, we showed that Mycn-T58M induced Ccnd1 and Ccnd2 expression upon its protein stability. We therefore investigated whether the increased expression level of Mycn affects corticogenesis by assessing its effect on neurogenesis in mouse neuronal progenitor/stem cells in the ventricular (VZ) or

subventricular/intermediate (SVZ/IZ) zones. Cells were triple stained for EdU, GFP and Ki67, a marker for all active phases of the cell cycle except the quiescent G0 state. Cells that remained proliferating after EdU incorporation were identified as EdU/Ki67 double-positive, while neurons that differentiated after EdU incorporation were EdU-positive but Ki67-negative (Fig.5A). Wild-type Mycn promoted cell cycle progression in the SVZ/IZ (Fig.5B) (Two-sided Student's *t*-test; $P < 0.01$; Empty; n=5; WT; n=4). Wild-type Mycn also tended to increase the number of EdU/Ki67 double-positive cells in the VZ, but this increase was not statistically significant.

We next sought to study the consequences of overexpression of wild-type Mycn for neuronal positioning. We electroporated *Mycn* constructs in combination with EGFP reporter construct into the VZ of E14.5 mouse neocortices and analyzed at P0. In P0 brain sections, we observed that neurons electroporated with the empty vector reached the superficial layers II-IV of the cortical plate (Fig.5C). However, electroporation of wild-type Mycn induced arrest of cells within layers V-VI (Two-sided Student's *t*-test; $P < 0.05$ for layers II-IV and layers V-VI; Empty; n=3; WT; n=3). In addition, Mycn-T58M affected cell proliferation and migration equally to wild-type Mycn (data not shown).

DISCUSSION

To our knowledge, this is the first report of a germline pathological gain-of-function missense mutation in *MYCN* (c.173C>T; p.Thr58Met), that may cause a megalencephaly syndrome with ID, ventriculomegaly, hypoplastic corpus callosum, distinctive facies, postaxial polydactyly and neuroblastoma. We show that MYCN-T58M functions in an unphosphorylated form with increased stability, leading to excess accumulation of the protein. Moreover, Mycn-T58M promoted the expression of Ccnd1 and Ccnd2 more significantly than wild-type Mycn, strongly suggesting that neuronal progenitor cells expressing Mycn-T58M are more proliferative than control cells *in vivo*. Ala replacement at Thr58 in Mycn has been shown to have transactivation capacity and enhanced stability, equivalent to the T58M substitution[25]. Furthermore, heterozygous mutations that stabilize CCND2 cause MPPH[11]. In this context, comparison of clinical features of the present patient to those of MPPH patients with *CCND2* mutations revealed common phenotypes, including ID, megalencephaly, ventriculomegaly, and postaxial polydactyly (Table 1). We assume that aberrant MYCN-CCND signaling is responsible for these shared clinical features.

Physiological MYCN activity is controlled via its regulated expression through sequential phosphorylation at S62 and T58. Phosphorylation at S62 by CDK1 via the Ras-Erk pathway

confers resistance to proteolysis and thus maintains the transcriptional activity[14]. This phosphorylation primes the subsequent phosphorylation at T58 by GSK3β via the PI3K-AKT pathway[13]. As a result, cells become highly sensitive to ubiquitination by Fbw7[16, 31]. On the other hand, since MYCN-T58M does not undergo the second phosphorylation, it is resistant to degradation by the ubiquitin-proteasome system, resulting in accumulation of the mutant protein followed by increased CCND1/2 expression.

Like other reported gene mutations causing MPPH, the p.T58M mutation in *MYCN* induces CCND2 expression and causes some similar clinical phenotypes. There are, however, some distinguishing features observed in the present patient. In one study, all reported MPPH patients with pathogenic mutations in *CCND2*, as well as in *AKT3, PIK3R2*, and *PIK3CA*, were complicated with polymicrogyria[32]. Whereas brain MRI did not detect polymicrogyria in the present case, abnormal cortical architecture could be seen by histopathological analysis, based on the result that expression of Mycn-T58M induced neuronal migration delay in fetal mouse neocortices. Additionally, the corpus callosum of the present patient was considerably thinner than that of MPPH patients. These discrepancies suggest the presence of yet unidentified MYCN-signaling pathways that are independently dysregulated in MPPH and the present case. Further analyses are required to clarify the molecular mechanisms underlying the clinical diversity.

Thirty seven loss-of-function abnormalities in *MYCN* have been listed in the HGMD to date[33]. These gene abnormalities cause Feingold syndrome and can be broken down into seven missense, six nonsense and 16 frame-shift mutations and eight gross deletions. Given that all the missense mutations were positioned in the basic-helix-loop-helix-Leucine zipper domain, transcriptional activity of MYCN should be attenuated through impaired DNA-binding[8, 34, 35]. Indeed, Feingold syndrome is thought to be caused by *MYCN* loss-of-function that results in a variety of symptoms, such as microcephaly and short stature[8, 36]. The HGMD also includes three gross insertions that exert pathological gain-of-function effects leading to tumors such as neuroblastoma and Wilms' tumor[33]. Notably, two of the three cases with gross insertions showed additional clinical features other than tumors. In addition to developmental delay, distinctive facial features are common symptoms, one showed postaxial polydactyly and the other presented ventriculomegaly, agenesis of the corpus callosum and ventricular septal defect [37-39].

Our data indicates that c.173C>T (p.Thr58Met) in *MYCN* exerts gain-of-function effects via increased protein stability and increased neuronal proliferation. Since the patient in this study presented phenotypes similar to those of patients with *MYCN* duplication[37, 39], we assume that expression of both wild-type Mycn and Mycn-T58M could facilitate neuronal progenitor cell proliferation. Thus, the sharp contrast in clinical phenotypes between the

present case and those diagnosed with Feingold syndrome is likely to be derived from upregulation of the MYCN-CCND-mediated transcription pathway in the former, and downregulation of the pathway in the latter (Table 1).

Given that Mycn-T58M is thought to have gain-of-function effects, overexpression of wild type Mycn should mimic the mutation phenotypes in developing cerebral cortex. Indeed, cortical neuron proliferation was facilitated by exogenous Mycn in the SVZ and IZ, but not in the VZ where apical progenitor cells (radial glia) accumulate. This may correlate with the dominant distribution of CCND2-positive cells in the SVZ rather than the VZ[40]. Neuronal progenitor cells in the SVZ and IZ are categorized as basal progenitors essential for the human-specific development of neocortex[41]. Thus, dysregulated MYCN-CCND2 function is possibly involved in megalencephaly and microcephaly in human diseases. The electroporation method used in this study results in different expression levels of protein among cells, dependent on the amount of incorporated expression vector. Our experiments showed that introduction of high levels of Mycn into neuronal progenitor cells appeared to cause cell death *in vitro*. Because of this non-uniformity of gene expression, cells overexpressing Mycn might have died and the result of our experiment appears not to reflect the accurate proliferative function of Mycn-T58M. We assume that subtle or moderate transcriptional activity by exogenous Mycn is enough to accelerate neurogenesis

in the SVZ and IZ, since *MYCN* duplication also gives rise to similar clinical features[37, 39]. From these results, we consider that the expression level of Mycn may determine cell fate, proliferation or cell death; low to moderate Mycn expression promotes cell proliferation whereas high expression results in cell cycle arrest followed by cell death. Therefore, gain-of-function effects of the MYCN-T58M mutant with increased stability may be enough to accelerate neurogenesis equivalent to that of duplication of the entire MYCN and cause megalencephaly via excess production of neuronal cells during corticogenesis.

In summary, we identified a *de novo* gain-of-function heterozygous missense mutation in *MYCN* in a patient with a novel megalencephaly syndrome similar to, but distinct from, PI3K-AKT-CCND2-related MPPH. This finding, and our subsequent functional analysis of the mutation, provides new insight into the critical role of MYCN in brain development.

Acknowledgments

The authors thank the patient and his parents for participating in this study.

Contributors

SS was responsible for the concept and design of the study. K Kato, KN, and SS drafted the main manuscript. K Kato, FM, NH, YN, HI, IH, KN, and SS analyzed and interpreted the data.

KKato, YK, HO, and SS contributed clinical data. AH, NO, MK, TT, YK, K Kosaki, and YT revised the manuscript and made comments on the structure, details and grammar of the article.

Funding

This study was partially supported by JSPS KAKENHI Grant Number JP16K15530 (SS), and by the Program for an Integrated Database of Clinical and Genomic Information from the Japanese Agency for Medical Research and Development, AMED (SS).

Competing Interests None declared.

Patient consent Obtained.

Ethics approval

This study was approved by the institutional review board of Nagoya City University Graduate School of Medical Sciences.

REFERENCES

1. Bretones G, Delgado MD, Leon J. Myc and cell cycle control. Biochim Biophys Acta 2015;1849:506-16.
2. Gustafson WC, Weiss WA. Myc proteins as therapeutic targets. Oncogene 2010;29:1249-59.
3. Stanton BR, Perkins AS, Tessarollo L, Sassoon DA, Parada LF. Loss of N-myc function results in embryonic lethality and failure of the epithelial component of the embryo to develop. Genes Dev 1992;6:2235-47.
4. Zindy F, Knoepfler PS, Xie S, Sherr CJ, Eisenman RN, Roussel MF. N-Myc and the cyclin-dependent kinase inhibitors p18Ink4c and p27Kip1 coordinately regulate cerebellar development. Proceedings of the National Academy of Sciences of the United States of America 2006;103:11579-83.
5. Ota S, Zhou ZQ, Keene DR, Knoepfler P, Hurlin PJ. Activities of N-Myc in the developing limb link control of skeletal size with digit separation. Development 2007;134:1583-92.
6. Moens CB, Stanton BR, Parada LF, Rossant J. Defects in heart and lung development in compound heterozygotes for two different targeted mutations at the N-myc locus. Development 1993;119:485-99.
7. Grady EF, Schwab M, Rosenau W. Expression of N-myc and c-src during the development of fetal human brain. Cancer research 1987;47:2931-6.
8. Marcelis CL, Hol FA, Graham GE, Rieu PN, Kellermayer R, Meijer RP, Lugtenberg D, Scheffer H, van Bokhoven H, Brunner HG, de Brouwer AP. Genotype-phenotype correlations in MYCN-related Feingold syndrome. Hum Mutat 2008;29:1125-32.
9. Cognet M, Nougayrede A, Malan V, Callier P, Cretolle C, Faivre L, Genevieve D, Goldenberg A, Heron D, Mercier S, Philip N, Sigaudy S, Verloes A, Sarnacki S, Munnich A, Vekemans M, Lyonnet S, Etchevers H, Amiel J, de Pontual L. Dissection of the MYCN locus in Feingold syndrome and isolated oesophageal atresia. Eur J Hum Genet 2011;19:602-6.
10. Ciemerych MA, Kenney AM, Sicinska E, Kalaszczynska I, Bronson RT, Rowitch DH, Gardner H, Sicinski P. Development of mice expressing a single D-type cyclin. Genes Dev 2002;16:3277-89.
11. Mirzaa G, Parry DA, Fry AE, Giamanco KA, Schwartzentruber J, Vanstone M, Logan CV, Roberts N, Johnson CA, Singh S, Kholmanskikh SS, Adams C, Hodge RD, Hevner RF, Bonthron DT, Braun KPJ, Faivre L, Riviere JB, St-Onge J, Gripp KW, Mancini GM, Pang K, Sweeney E, van Esch H, Verbeek N, Wieczorek D, Steinraths

M, Majewski J, Consortium FC, Boycot KM, Pilz DT, Ross ME, Dobyns WB, Sheridan EG. De novo CCND2 mutations leading to stabilization of cyclin D2 cause megalencephaly-polymicrogyria-polydactyly-hydrocephalus syndrome. Nat Genet 2014;46:510-15.

12. Riviere JB, Mirzaa GM, O'Roak BJ, Beddaoui M, Alcantara D, Conway RL, St-Onge J, Schwartzentruber JA, Gripp KW, Nikkel SM, Worthylake T, Sullivan CT, Ward TR, Butler HE, Kramer NA, Albrecht B, Armour CM, Armstrong L, Caluseriu O, Cytrynbaum C, Drolet BA, Innes AM, Lauzon JL, Lin AE, Mancini GM, Meschino WS, Reggin JD, Saggar AK, Lerman-Sagie T, Uyanik G, Weksberg R, Zirn B, Beaulieu CL, Finding of Rare Disease Genes Canada C, Majewski J, Bulman DE, O'Driscoll M, Shendure J, Graham JM, Jr., Boycott KM, Dobyns WB. De novo germline and postzygotic mutations in AKT3, PIK3R2 and PIK3CA cause a spectrum of related megalencephaly syndromes. Nat Genet 2012;44:934-40.
13. Sears R. Multiple Ras-dependent phosphorylation pathways regulate Myc protein stability. Genes & Development 2000;14:2501-14.
14. Sjostrom SK, Finn G, Hahn WC, Rowitch DH, Kenney AM. The Cdk1 complex plays a prime role in regulating N-myc phosphorylation and turnover in neural precursors. Developmental cell 2005;9:327-38.
15. Welcker M, Orian A, Grim JE, Eisenman RN, Clurman BE. A nucleolar isoform of the Fbw7 ubiquitin ligase regulates c-Myc and cell size. Curr Biol 2004;14:1852-7.
16. Yada M, Hatakeyama S, Kamura T, Nishiyama M, Tsunematsu R, Imaki H, Ishida N, Okumura F, Nakayama K, Nakayama KI. Phosphorylation-dependent degradation of c-Myc is mediated by the F-box protein Fbw7. EMBO J 2004;23:2116-25.
17. Bahram F, von der Lehr N, Cetinkaya C, Larsson LG. c-Myc hot spot mutations in lymphomas result in inefficient ubiquitination and decreased proteasome-mediated turnover. Blood 2000;95:2104-10.
18. Negishi Y, Miya F, Hattori A, Johmura Y, Nakagawa M, Ando N, Hori I, Togawa T, Aoyama K, Ohashi K, Fukumura S, Mizuno S, Umemura A, Kishimoto Y, Okamoto N, Kato M, Tsunoda T, Yamasaki M, Kanemura Y, Kosaki K, Nakanishi M, Saitoh S. A combination of genetic and biochemical analyses for the diagnosis of PI3K-AKT-mTOR pathway-associated megalencephaly. BMC Med Genet 2017;18:4.
19. Ito H, Mizuno M, Noguchi K, Morishita R, Iwamoto I, Hara A, Nagata KI. Expression analyses of Phactr1 (phosphatase and actin regulator 1) during mouse brain development. Neuroscience research 2018;128:50-57.
20. Hamada N, Iwamoto I, Tabata H, Nagata KI. MUNC18-1 gene abnormalities are involved in neurodevelopmental disorders through defective cortical architecture

during brain development. Acta neuropathologica communications 2017;5:92.

21. Hamada N, Ito H, Iwamoto I, Morishita R, Tabata H, Nagata K. Role of the cytoplasmic isoform of RBFOX1/A2BP1 in establishing the architecture of the developing cerebral cortex. Mol Autism 2015;6:56.
22. Kanda Y. Investigation of the freely available easy-to-use software 'EZR' for medical statistics. Bone marrow transplantation 2013;48:452-8.
23. Brodeur GM, Pritchard J, Berthold F, Carlsen NL, Castel V, Castelberry RP, De Bernardi B, Evans AE, Favrot M, Hedborg F, et al. Revisions of the international criteria for neuroblastoma diagnosis, staging, and response to treatment. Journal of clinical oncology : official journal of the American Society of Clinical Oncology 1993;11:1466-77.
24. Aoki S, Hashimoto K, Ikeda N, Takekoh M, Fujiwara T, Morisaki N, Mezawa H, Tachibana Y, Ohya Y. Comparison of the Kyoto Scale of Psychological Development 2001 with the parent-rated Kinder Infant Development Scale (KIDS). Brain & development 2016;38:481-90.
25. Kenney AM, Widlund HR, Rowitch DH. Hedgehog and PI-3 kinase signaling converge on Nmyc1 to promote cell cycle progression in cerebellar neuronal precursors. Development 2004;131:217-28.
26. Kenney AM. Nmyc upregulation by sonic hedgehog signaling promotes proliferation in developing cerebellar granule neuron precursors. Development 2003;130:15-28.
27. Pontious A, Kowalczyk T, Englund C, Hevner RF. Role of intermediate progenitor cells in cerebral cortex development. Developmental neuroscience 2008;30:24-32.
28. Nonaka-Kinoshita M, Reillo I, Artegiani B, Martinez-Martinez MA, Nelson M, Borrell V, Calegari F. Regulation of cerebral cortex size and folding by expansion of basal progenitors. EMBO J 2013;32:1817-28.
29. Murphy DJ, Junttila MR, Pouyet L, Karnezis A, Shchors K, Bui DA, Brown-Swigart L, Johnson L, Evan GI. Distinct thresholds govern Myc's biological output in vivo. Cancer Cell 2008;14:447-57.
30. Ushmorov A, Hogarty MD, Liu X, Knauss H, Debatin KM, Beltinger C. N-myc augments death and attenuates protective effects of Bcl-2 in trophically stressed neuroblastoma cells. Oncogene 2008;27:3424-34.
31. Xiao D, Yue M, Su H, Ren P, Jiang J, Li F, Hu Y, Du H, Liu H, Qing G. Polo-like Kinase-1 Regulates Myc Stabilization and Activates a Feedforward Circuit Promoting Tumor Cell Survival. Mol Cell 2016;64:493-506.
32. Mirzaa G. MPPH Syndrome. In: Adam MP, Ardinger HH, Pagon RA, Wallace SE, Bean LJH, Stephens K, Amemiya A, eds. GeneReviews((R)). Seattle (WA): University of

Washington, Seattle

University of Washington, Seattle. GeneReviews is a registered trademark of the University of Washington, Seattle. All rights reserved., 1993.

33. Stenson PD, Ball EV, Mort M, Phillips AD, Shiel JA, Thomas NS, Abeysinghe S, Krawczak M, Cooper DN. Human Gene Mutation Database (HGMD): 2003 update. Hum Mutat 2003;21:577-81.
34. Chaudhary J, Skinner MK. Basic helix-loop-helix proteins can act at the E-box within the serum response element of the c-fos promoter to influence hormone-induced promoter activation in Sertoli cells. Molecular endocrinology (Baltimore, Md) 1999;13:774-86.
35. van Bokhoven H, Celli J, van Reeuwijk J, Rinne T, Glaudemans B, van Beusekom E, Rieu P, Newbury-Ecob RA, Chiang C, Brunner HG. MYCN haploinsufficiency is associated with reduced brain size and intestinal atresias in Feingold syndrome. Nat Genet 2005;37:465-7.
36. Celli J, van Bokhoven H, Brunner HG. Feingold syndrome: clinical review and genetic mapping. Am J Med Genet A 2003;122a:294-300.
37. Van Mater D, Knelson EH, Kaiser-Rogers KA, Armstrong MB. Neuroblastoma in a pediatric patient with a microduplication of 2p involving the MYCN locus. Am J Med Genet A 2013;161A:605-10.
38. Fievet A, Belaud-Rotureau MA, Dugay F, Abadie C, Henry C, Taque S, Andrieux J, Guyetant S, Robert M, Dubourg C, Edan C, Rioux-Leclercq N, Odent S, Jaillard S. Involvement of germline DDX1-MYCN duplication in inherited nephroblastoma. Eur J Med Genet 2013;56:643-7.
39. Micale MA, Embrey Bt, Macknis JK, Harper CE, Aughton DJ. Constitutional 560.49 kb chromosome 2p24.3 duplication including the MYCN gene identified by SNP chromosome microarray analysis in a child with multiple congenital anomalies and bilateral Wilms tumor. Eur J Med Genet 2016;59:618-23.
40. Glickstein SB, Alexander S, Ross ME. Differences in cyclin D2 and D1 protein expression distinguish forebrain progenitor subsets. Cereb Cortex 2007;17:632-42.
41. Florio M, Huttner WB. Neural progenitors, neurogenesis and the evolution of the neocortex. Development 2014;141:2182-94.

FIGURE LEGENDS

Figure 1. Clinical features of the patient

(A and B) Distinctive facial features were observed, including prominent forehead, thick and laterally extended eyebrow, posteriorly rotated ear, epicanthus, hypertelorism, wide and depressed nasal bridge, wide nasal base, upturned nasal tip, long philtrum and square face. (C) X-ray image showing postaxial polydactyly. (D and E) Axial slices of T2-weighted images acquired at 15 years show ventriculomegaly, but no polymicrogyria. (F) Sagittal slice of T2-weighted image taken at 17 months of age showing hypoplastic corpus callosum. The patient's parents gave written consent for publication of the photographs.

Figure 2. Genetic analysis of the patient.

(A) The data analysis algorithm used for filtering all single nucleotide variants identified using trio-based whole-exome sequence, with the number of remaining variants after each filtering step. Upon filtering and prioritization, a *de novo* heterozygous missense mutation (c.173C>T; p.Thr58Met) in *MYCN* was identified as the top candidate. (B) Pedigree analyses with the patient represented by a filled symbol. The genotype of the variant p.Thr58Met or wild-type (WT) in the *MYCN* gene is given. (C) Genomic DNA sequence chromatograms indicating the position of the c.173C>T mutation. (D) Phylogenic

conservation was observed for the mutated amino acid residue, marked by an asterisk.

Figure 3. Expression profile of Mycn protein during mouse brain development.

Tissue extracts of whole-brain (E13.5, E15.5, E17.5, P0) and cerebral cortices (P3, P8, P15, P30) were subjected to western blotting with an anti-N-Myc antibody. Anti-Sept11 was used as a loading control.

Figure 4. Effects of the p.T58M mutation on Mycn stability and Ccnd expression in neuronal progenitor/stem cells

(A) Expression of MYCN, MYCN-T58M, and MYCN-P44L in HEK293T cells. Lysates from cells expressing MYCN, MYCN-T58M, or MYCN-P44L were subjected to SDS-PAGE followed by western blotting with anti-N-Myc, phospho-c-Myc (pThr58), phospho-n-Myc (pSer62) or GAPDH antibodies. GAPDH immunoreactivity indicates equivalent loading. Anti-phosphorylated-c-Myc (pThr58) antibody recognized wild-type MYCN, but not MYCN-T58M. In contrast, MYCN-P44L mutant was associated with significantly increased levels of MYCN forms phosphorylated at Thr58 and Ser62. Fold change of phosphorylated MYCN level with respect to MYCN expression level was normalized to MYCN-WT from three independent experiments. (B) Expression of Mycn and Mycn-T58M in neuronal

progenitor/stem cells in the presence (*left* two lanes) or absence (*right* two lanes) of Fbw7. Quantification of Mycn levels as a proportion of GFP levels averaged over three independent experiments. Relative densities of the bands were determined relative to 1 for wild-type. Electroporation with Mycn-T58M caused an accumulation of mutant protein compared to wild-type. (C) Western blotting of Mycn and Mycn-T58M in neuronal progenitor/stem cells. Quantification was performed as in (B). Mycn levels as a proportion of Gapdh levels averaged over six independent experiments. Mycn-T58M was expressed at levels much higher than wild-type at 72 h. (D) Expression of Ccnd1 and Ccnd2 in neuronal progenitor/stem cells transfected with control pCAG (Empty), pCAG-Myc-Mycn (WT) or pCAG-Myc-Mycn-T58M, together with pCAG-EGFP. Quantification was done as in (B). Protein levels as a proportion of Gapdh levels averaged over six independent experiments. Significantly higher expression was observed in cells expressing Mycn-T58M at 72 h. Bar graphs, B–D, means and s.e.m. are shown; * $P < 0.05$, ** $P < 0.01$.

Figure 5. Effect of Mycn overexpression on cell cycle and migration in neuronal progenitor/stem cells

(A) E14.0 cortices were co-electroporated with pCAG-EGFP together with pCAG-Myc (Empty) or pCAG-Myc-Mycn-WT (WT) and coronal sections immunostained for GFP (green), EdU (red) and Ki67 (Blue). GFP/EdU/Ki67 triple-positive cells are indicated by

arrowheads. Scale bar, 10μm. (B) Quantification of GFP/EdU/Ki67 triple-positive cells relative to GFP/EdU double-positive ones in (A). Wild-type Mycn promoted cell cycle progression in the SVZ/IZ. (C) In utero transfection was done as in (A), followed by fixation at P0. Coronal sections of samples transfected with Empty (control) or wild-type Mycn were immunostained for GFP. (D) Quantification of the distribution of transfected neurons in distinct parts of the cerebral cortex for each condition shown in (C). (B, D) Bar graph, means and s.e.m. are shown; * $P < 0.05$, ** $P < 0.01$.

Supplementary Figure 1. The efficiency of electroporation

Neuronal progenitor/stem cells were co-electroporated with pCAG-EGFP and pCAG-Myc-Fbw7 together with pCAG-Myc-Mycn-WT or pCAG-Myc-Mycn-T58M. Western blotting of Mycn, Fbw7, β Actin, and GFP at 24 h after electroporation indicated equal amount of EGFP was transfected. β Actin immunoreactivity indicates equivalent loading.

Table 1. Comparison of clinical features in the present patient, and patients with Feingold syndrome or MPPH

	Patient 1	Feingold syndrome	MPPH
Intellectual disability	severe	mild learning deficiency	mild to severe
Postnatal growth retardation	+	+	−
Skull	macrocephaly	microcephaly	macrocephaly
Brain MRI findings			
Ventriculomegaly	+	−	+
Bilateral perisylvian polymicrogyria	−	−	+
Corpus callosum dysplasia	hypoplastic	−	thick or mega
Congenital heart disease	VSD	±	±
Digital anomalies			
Postaxial polydactyly	+	−	+
Toe syndactyly	−	+	−
Brachymesophalangy	−	+	−
Tracheal dysplasia	tracheomalacia	tracheoesophageal fistula	−
Gastrointestinal atresia	−	±	−

MPPH; megalencephaly-polymicrogyria-polydactyly-hydrocephalus syndrome, VSD; ventricular septal defect, +; present, −; absent, ±; occasional

Fig.1

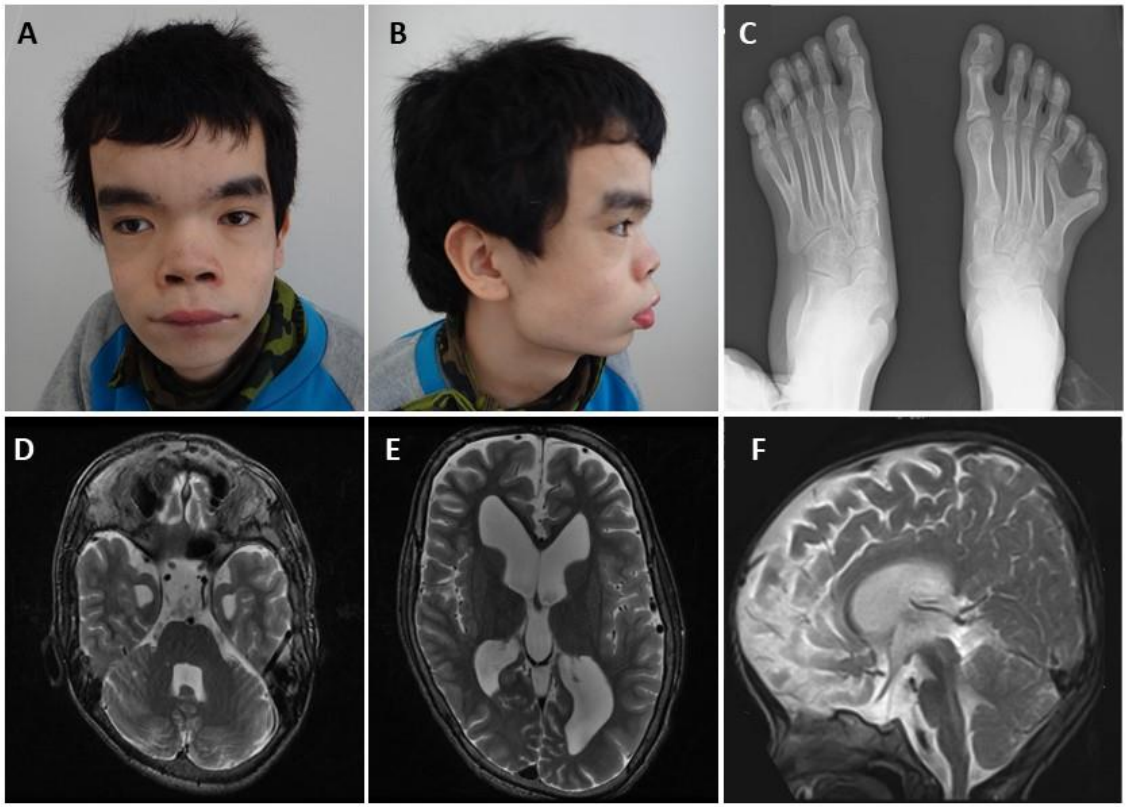

Fig.2

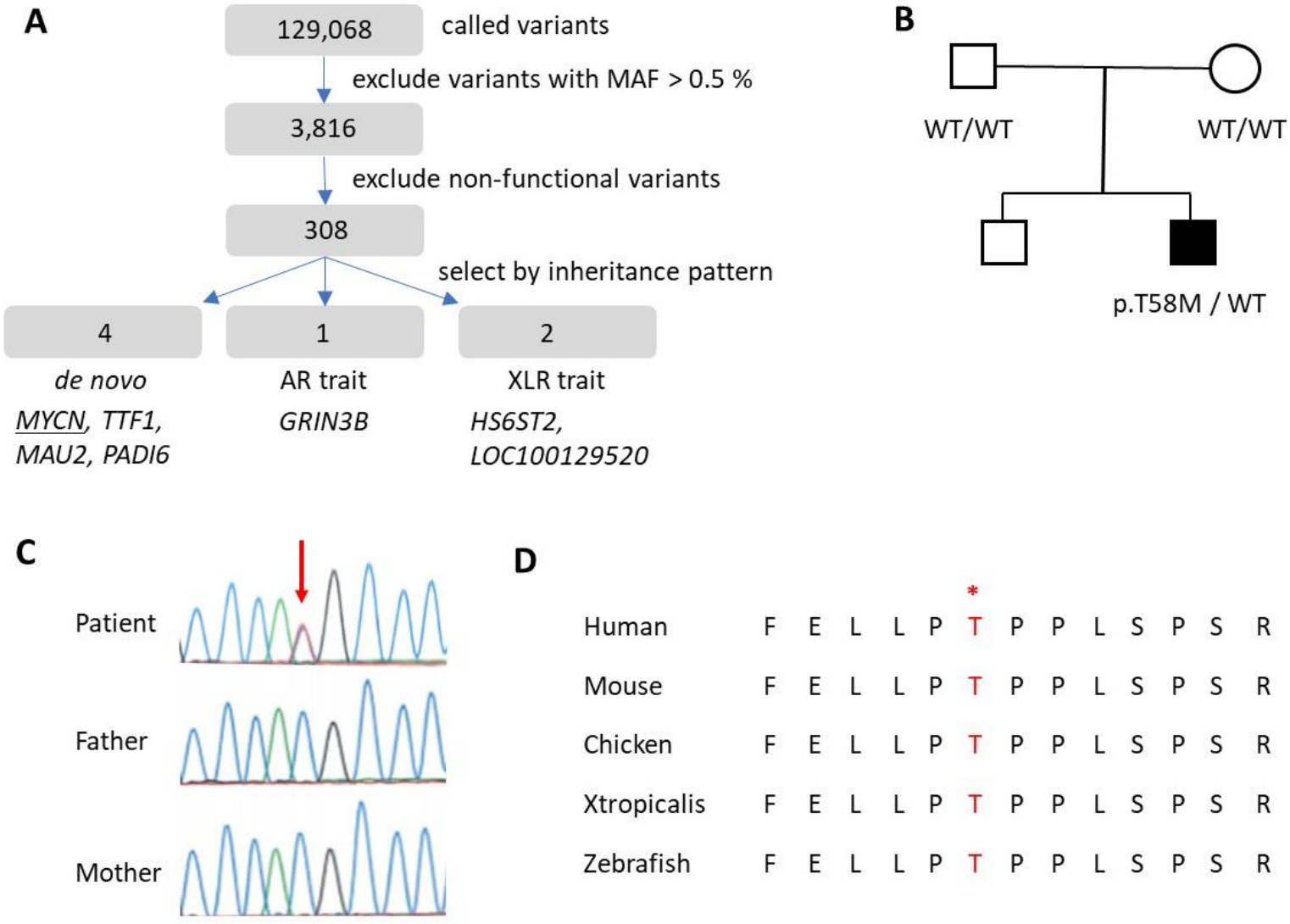
A
129,068
called variants
exclude variants with MAF > 0.5 %
3,816
exclude non-functional variants
308
select by inheritance pattern
4
1
2
de novo
AR trait
XLR trait
MYCN, TTF1, MAU2, PADI6
GRIN3B
HS6ST2, LOC100129520
B
WT/WT
WT/WT
p.T58M / WT
C
Patient
Father
Mother
D
Human F E L L P T P P L S P S R
Mouse F E L L P T P P L S P S R
Chicken F E L L P T P P L S P S R
Xtropicalis F E L L P T P P L S P S R
Zebrafish F E L L P T P P L S P S R

Fig.3

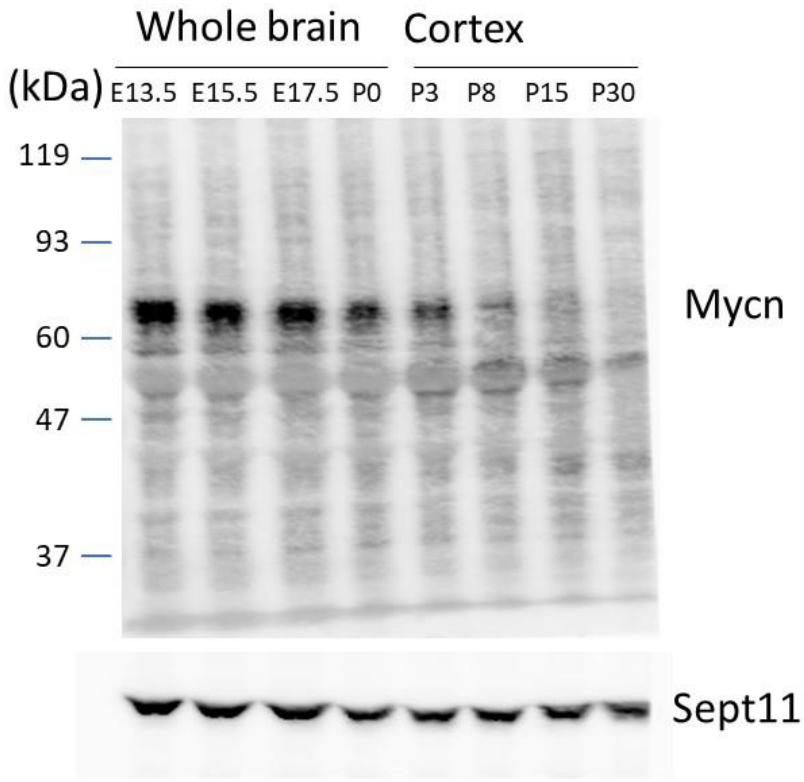
Whole brain
Cortex
(kDa)
E13.5
E15.5
E17.5
P0
P3
P8
P15
P30
119
93
60
47
37
Mycn
Sept11

Fig.4

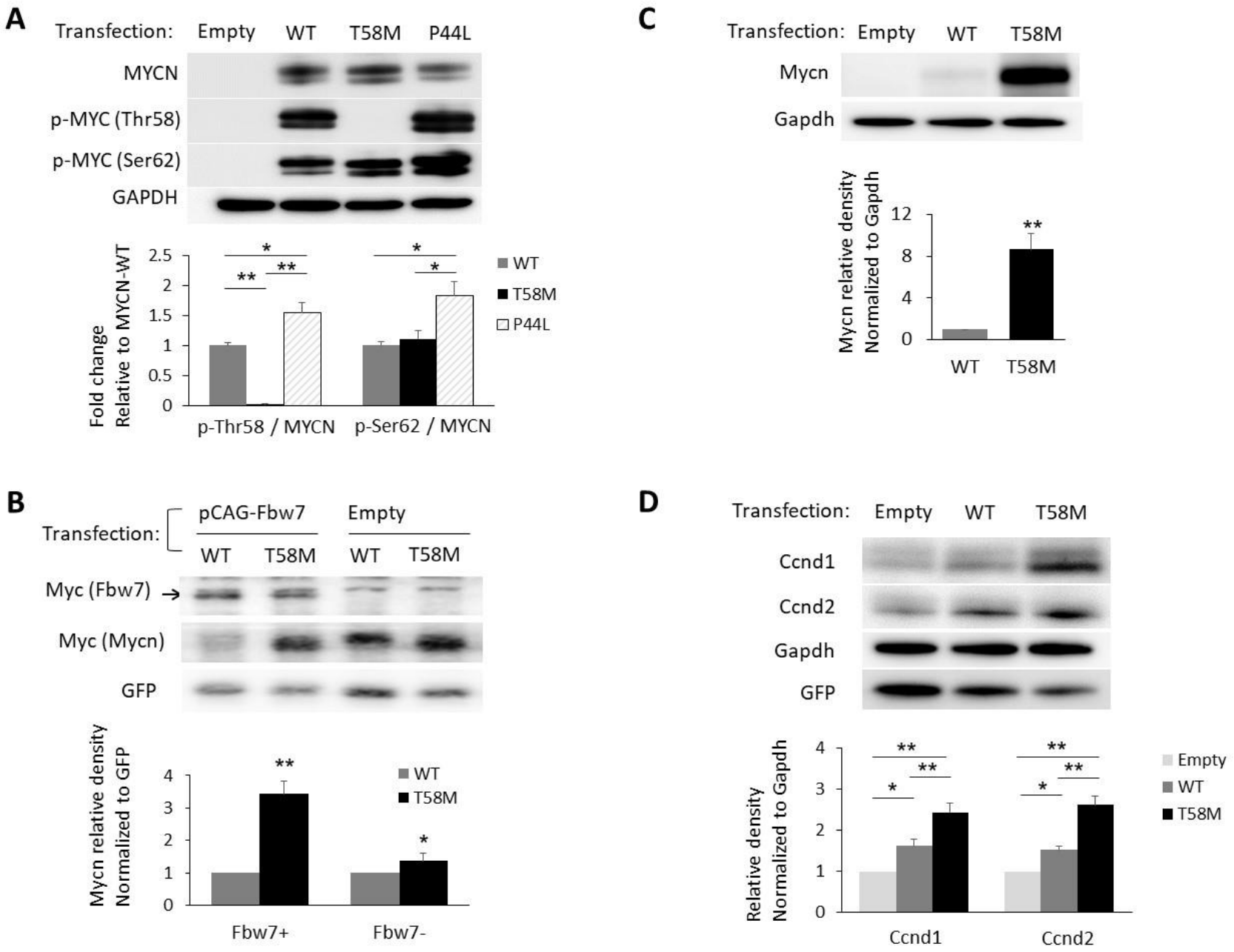
A
Transfection: Empty WT T58M P44L
MYCN
p-MYC (Thr58)
p-MYC (Ser62)
GAPDH
Fold change Relative to MYCN-WT
WT
T58M
P44L
p-Thr58 / MYCN
p-Ser62 / MYCN
B
Transfection: pCAG-Fbw7 Empty
WT T58M WT T58M
Myc (Fbw7)
Myc (Mycn)
GFP
Mycn relative density Normalized to GFP
Fbw7+
Fbw7-
C
Transfection: Empty WT T58M
Mycn
Gapdh
Mycn relative density Normalized to Gapdh
WT
T58M
D
Transfection: Empty WT T58M
Ccnd1
Ccnd2
Gapdh
GFP
Relative density Normalized to Gapdh
Empty
WT
T58M
Ccnd1
Ccnd2

Fig.5

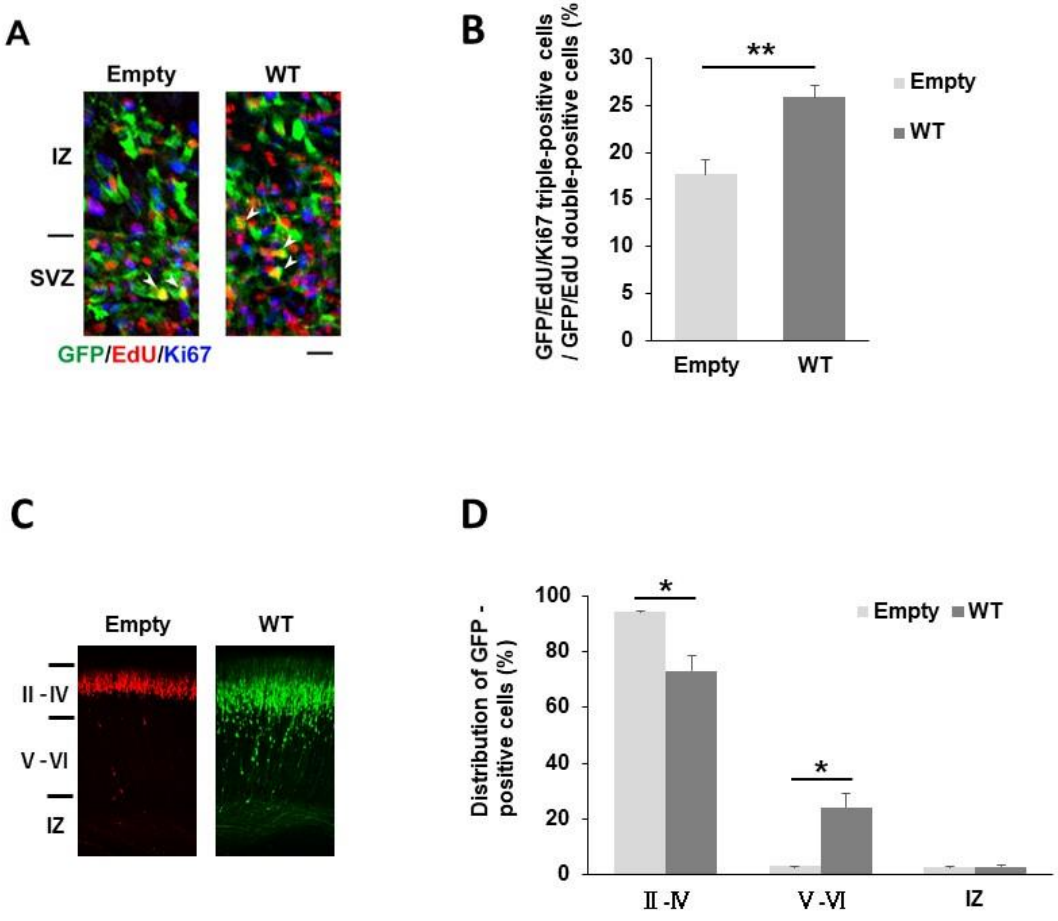
A
Empty
WT
IZ
SVZ
GFP/EdU/Ki67
B
GFP/EdU/Ki67 triple-positive cells / GFP/EdU double-positive cells (%)
**
Empty
WT
C
Empty
WT
II - IV
V - VI
IZ
D
Distribution of GFP - positive cells (%)
*
*
Empty
WT
II -IV
V -VI
IZ

Supplementary Fig.1